Modeling the Impacts of a Man-Made Lake on the Meteorological Conditions of the Surrounding Areas

Klaić, Zvjezdana B.; Kvakić, Marko

Modeling the Impacts of a Man-Made Lake on the Meteorological Conditions of the Surrounding Areas

ZVJEZDANA B. KLAIĆ

Andrija Mohorovičić Geophysical Institute, Department of Geophysics, Faculty of Science, University of Zagreb, Zagreb, Croatia

MARKO KVAKIĆ

Météo-France, Centre National de Recherches Météorologiques, Toulouse, France

(Manuscript received 14 May 2013, in final form 29 November 2013)

ABSTRACT

The possible modifications of the surface meteorological conditions due to construction of a small, man-made lake in midlatitudes (surface area of 11.55 km^2 and maximum fetch distance $L \approx 5$ km) were investigated using the Weather Research and Forecasting (WRF) model (version 3.3). The model was applied to four real typical synoptic situations for which the area of interest was under the influence of a wintertime anticyclone (WA), a wintertime cyclone (WC), a summertime anticyclone (SA), and a summertime cyclone (SC). Each of these four typical synoptic setups was simulated twice—once assuming the present state (''NO-LAKE'' experiment) and again assuming the existence of the new lake (''LAKE'' experiment). The differences between 36-h average LAKE and NO-LAKE simulation results show noticeable mean changes in the surface temperature and relative humidity as well as a small increase of the mean surface wind speeds in the air above the newly constructed lake. At other portions of the investigated area (distances up to ~4L–6L downstream of the new lake), the 36-h mean differences produced by the new lake are below the order of magnitude of accuracy of operational meteorological measurement instruments. In individual hours, however, these differences are occasionally very high, particularly for cyclonic episodes. In addition, results obtained for SA suggest an existence of a lake circulation cell associated with small differences between the lake and land temperatures (at most up to ~3°–5°C) and consequently, a slight enhancement of slope winds in future (LAKE) conditions.

1. Introduction

Man-made lakes affect the environment in many ways. Some of these effects are landscape and land-use/land-cover changes, loss of habitat for existing species due to flooding, and settlement of the new inhabitants in the flooded area (e.g., Dale et al. 2011). Man-made lakes can also change groundwater levels and, consequently, cause a decline of ambient species sensitive to groundwater level disturbances (e.g., Antonić et al. 2001). Additionally, any alteration of the land use/land cover will change the surface roughness as well as the heat and moisture fluxes at the earth's surface, thus modifying local weather conditions (e.g., Klaić et al. 2002) and climate (e.g., Foley et al. 2005; Bazgeer et al. 2008; Hernández et al. 2012).

During the past decade, a number of studies investigating impacts of midlatitude lakes on ambient meteorological conditions focused on the wintertime lake-effect precipitation events. Such events are associated with meso-β-scale circulations that develop because of cold air moving over a warmer lake (e.g., Laird et al. 2003a), and they can produce heavy snowfalls (e.g., Cordeira and Laird 2008). Investigations of wintertime lake-effect precipitation events can be grouped as follows: 1) *Mesoscale numerical modeling studies of the morphology of the lake-effect circulations over idealized lakes*. These studies point to the importance of the ratio of wind speed U to maximum fetch distance L in determining the morphology of lake-effect circulation for both circular (Laird et al. 2003a) and elliptical (Laird et al. 2003b) lakes. They also show that fields produced in simulations with elliptical lakes exhibit

Corresponding author address: Z. B. Klaić, Andrija Mohorovičić Geophysical Institute, Department of Geophysics, Faculty of Science, University of Zagreb, Horvatovac 95, Zagreb 10000, Croatia.
E-mail: zklaic@gfz.hr

DOI: 10.1175/JAMC-D-13-0163.1

more complex structures than those produced in simulations with circular lakes. 2) *Case studies of observed lake-effect precipitation events.* These studies report on the role of the land breezes in the development of the lake-effect snowband (Payer et al. 2007). Additionally, they show that the lake-effect snowstorms can develop in association with an extensively ice-covered lake (Cordeira and Laird 2008). 3) *Climatological analyses of lake-effect events*. These observational (Laird et al. 2009, 2010; Alcott et al. 2012; Workoff et al. 2012) and modeling (Notaro et al. 2013; Vavrus et al. 2013; Wright et al. 2013) studies focus on the frequency and environmental conditions favorable for the occurrence of lake-effect precipitation events. In addition, recent studies of the Finger Lakes (Laird et al. 2009, 2010) show that the lake-effect precipitation events can be initiated or enhanced by lakes that are much smaller (surface area ~10–100 km^2) than lakes previously considered as being associated with lake-effect events. However, such events do not produce snowfalls as considerable as the snowfalls associated with larger lakes.

Lake-breeze events over midlatitude lakes were also investigated. Harris and Kotamarthi (2005) performed mesoscale numerical simulations of two such events over Lake Michigan, focusing primarily on lake-breeze role in the dispersion of pollutants. Additionally, they inspected the sensitivity of modeled circulation to lake-surface temperatures. They obtained little change in the modeled breeze when measured lake-surface temperatures were used as initial and boundary conditions in the place of surface skin temperature (i.e., the temperature of the surface used to calculate the surface heat fluxes so that the sums of upward and downward fluxes are equal). Sills et al. (2011), while also addressing potential impact of the lake breezes on the air quality, identified lake-breeze events over the southern Great Lakes in 90% of days during June–August 2007. Occasionally, lake-breeze fronts penetrated as far as 200 km inland, which was confirmed by both observations and a high-resolution (2.5 km) numerical weather prediction model. In the review paper of numerical studies of both sea and lake breezes, Crosman and Horel (2010) pointed to the need for further investigations of the dependence of breezes on sets of basic configurations of water body dimensions, the area of heated land surface, coastline geometry, and surrounding topography. Recently, the same authors also performed large-eddy simulations of lake breezes for idealized lakes having diameters of 10, 25, 50, and 100 km (Crosman and Horel 2012). They concluded that the lake breezes for small lakes developed similarly to sea breezes in the morning, but had a significantly weaker horizontal wind speed component and a smaller horizontal extent than sea breezes in the afternoon. On the other hand, the lake breezes for large lakes (having diameters of 100 km) had characteristics similar to those for sea breezes in terms of sensitivity to heat flux and vertical stability. Finally, Asefi-Najafabady et al. (2012) recently analyzed Doppler radar observations of springtime lake-breeze circulations produced by a small lake. They showed that the lake-breeze circulation, once formed, can be persistent over a range of background wind flows despite the small lake size (mean width of ~2 km). However, the formation, location, strength, and inland penetration of the lake breeze were highly sensitive to the strength and direction of the background flow.

In this study, we investigate the possible impacts of a new man-made lake on the meteorological conditions of the surrounding areas. Specifically, a new hydropower plant is planned to be built in Lika-Senj County, Croatia. This project includes the construction of a new lake (Kosinj; surface area $1.155 \times 10^7\ m^2$, volume $3.3 \times 10^8\ m^3$, and maximum depth 30 m). The lake will be located adjacent to the existing one (Kruščica; surface area $8.6 \times 10^6\ m^2$, volume $1.4 \times 10^8\ m^3$, and maximum depth 38 m). Thus, both lakes will constitute a total storage volume of $4.7 \times 10^8\ m^3$. Here, we will inspect the effects of the alteration of a solid surface covered with vegetation by a water surface due to the new lake.

Four different typical large-scale (synoptic, i.e., horizontal length scale on the order of 1000 km) weather situations were simulated by the Weather Research and Forecasting (WRF) model, version 3.3 (Skamarock et al. 2008). Each of these four typical synoptic setups was simulated twice—once assuming the present state (''NO-LAKE'' experiment) and again assuming the existence of the new lake (''LAKE'' experiment). Possible modifications of meteorological conditions due to the construction of the new lake were thereafter assessed from the differences between meteorological fields obtained for the future and present state, that is, from the differences between meteorological fields obtained for the LAKE and NO-LAKE experiments.

The present modeling study differs from past investigations of lake influences in several respects. While previous studies were focused on specific seasonal mesoscale phenomena (either wintertime lake-effect precipitation event or summertime lake-breeze event), here we consider both cold and warm seasons. Additionally, modeling studies discussed above addressed either idealized (Laird et al. 2003a,b; Crosman and Horel 2012) or substantially larger real lakes (Harris and Kotamarthi 2005; Sills et al. 2011; Vavrus et al. 2013; Wright et al. 2013), whereas we look at a small, real lake. Other studies dealing with real lakes of comparable sizes are either climatological (Laird et al. 2009, 2010) or observational (Asefi-Najafabady et al. 2012). None of the

above studies addressed an alteration of a solid surface by a lake.

2. Model description

The WRF model (Skamarock et al. 2008) is a complex numerical weather prediction modeling system designed to simulate weather conditions at the mesoscale, that is, at the horizontal resolution of ~1 km. The model has been widely applied for both scientific and operational purposes (e.g., Skamarock and Klemp 2008; Coniglio et al. 2010; Horvath et al. 2012).

The WRF dynamics solver numerically integrates a system of flux-form prognostic equations (Euler equations) for air velocity components, potential temperature, geopotential, air pressure, and inverse air density (specific volume). The equation system is formulated using a terrain-following hydrostatic-pressure vertical coordinate and is thus suitable for applications over areas with complex topography. Furthermore, the Euler equations include moisture through mixing ratios for water vapor, cloud, rain, and ice, where the mixing ratio is defined as a mass of particular quantity per mass of dry air.

The model can be run with user-defined initial and boundary conditions (which are suitable for idealized simulations), or it can use the data from either an external analysis of measured fields or forecasts (suitable for real-data cases). The WRF modeling system also enables nested simulations, where the results obtained for the outer grid (at the coarser resolution) provide initial and boundary conditions for the inner grid (at the finer resolution).

The modeling system distinguishes five categories of physical parameterizations: microphysical, cumulus, planetary boundary layer, land surface model, and radiation parameterization. Several parameterization schemes are offered for each of these five categories [for full details, refer to Skamarock et al. (2008)].

3. Input data

a. Modeling domains

The new hydropower plant will be located in the Lika region, Lika-Senj County, Croatia (Fig. 1b). This region belongs to the wider area of the Dinaric karst (e.g., Biondić et al. 1998) and is characterized by a prevalently mountainous landscape with karst fields, known as *poljes* in the karst terminology (e.g., Nicod 2003). According to an evaluation of the entire county of Lika-Senj (Bogunović et al. 2013), forests occupy approximately 61.3% of the area, while the remaining 38.7% corresponds to agricultural land comprising pastures, meadows, plough land, karst orchards, and vineyards.

From the southwest, the Lika region is bounded by the Velebit mountain range (with a highest peak of 1757 m), which stretches along the shoreline and thus isolates the region from the thermal influence of the Adriatic Sea. Therefore, the Lika region has a mountain climate that differs from the wider area, mainly by its air temperature and snow regime (Zaninović et al. 2008).

To better represent complex topography and other surface characteristics of such a heterogeneous area, we performed double-nested simulations (Fig. 1a, Table 1) with three domains. The largest domain (d01; horizontal resolution of 9 km) was employed to produce initial and boundary conditions for the medium domain (d02; horizontal resolution of 3 km), while the medium domain was used to produce initial and boundary conditions for the innermost domain (d03; horizontal resolution of 1 km). Last, results obtained at the finest resolution (1 km; d03) were considered relevant.

All three domains have the same central point placed above the existing lake Kruščica (latitude 44.68°N, longitude 15.26°E, Fig. 1b), the same height (20 km above the ground), and the same vertical resolution. In the vertical, 49 layers were assumed, allowing for finer resolution at lower altitudes—layer depths gradually increased from 50 m at the bottom to several hundred meters at the top of the modeling domain.

As seen from Fig. 1b, the smallest domain, d03, is much larger than the area where we would expect the new lake to influence environmental conditions. Namely, based on results of mesoscale-model simulations of lake-effect circulations over idealized lakes (Laird et al. 2003a,b), we assume that influences of the new lake can extend downwind of the lake at most up to several maximum fetch distances. The horizontal dimensions of domain d03 are 120 km × 120 km (Table 1), while the surface of the future lake has an area of only 11.55 km^2 (Figs. 1b,c) and the maximum fetch distance is $L \approx 5$ km. Such a large domain of interest is selected to capture meteorological measuring sites, that is, to enable validation of the model performance at the wider region because there are no meteorological measuring sites in the vicinity of the lakes. In section 4, however, where we will discuss the model results, we will focus on a smaller area around the lakes (50 km × 50 km), which corresponds to distances up to ~20–30 km downwind of the new lake (i.e., ~4*L*–6*L*).

b. Other input data

Apart from the selection of simulated periods, which will be described in the next subsection, other input data that must be defined for each domain prior to any simulation are the model mask (the spatial distribution of water and land surfaces within the domain), the land-use distribution, the domain topography, and the selection

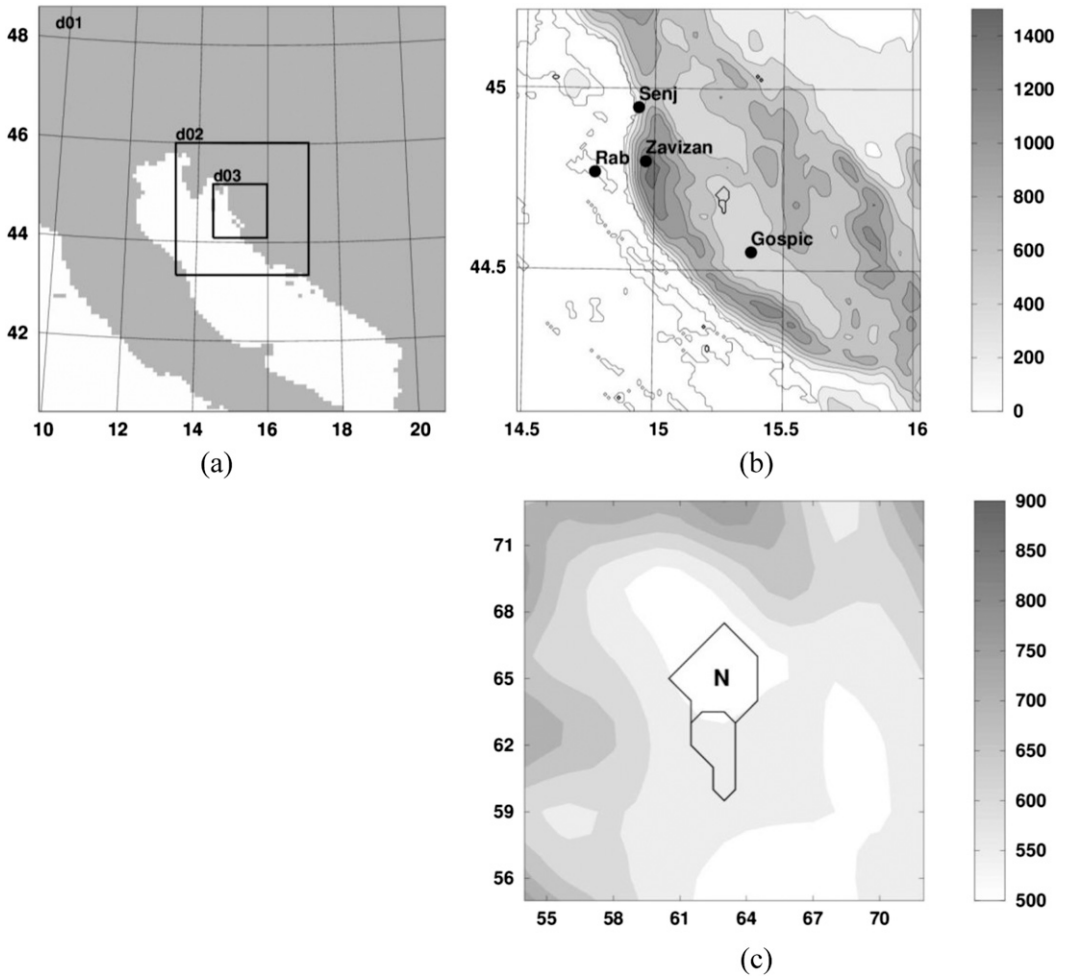

FIG. 1. (a) Three nested domains: d01 (891 km × 891 km), d02 (297 km × 297 km), and d03 (120 km × 120 km). (b) The smallest domain (d03). Positions of meteorological measuring sites (Senj, Rab, Zavižan, and Gospić) are indicated with black circles. Contours of two lakes are shown by the thick black lines in the center of the domain. Lakes are placed in the center of the domain d03. (c) A closer view of the future state with the two lakes (LAKE experiment). The future lake Kosinj is located north of the current lake and it is denoted by N. All three figures are shown in Lambert cylindrical projection. Here, (a) and (b) show the geographical latitude and longitude and (c) displays every third kilometer of the domain grid. Terrain topography (MSL) is shown in (b) and (c).

of numerical schemes and parameterizations. Additionally, initial and boundary conditions should be predetermined for the outermost domain.

For the current state (NO-LAKE experiment), model masks, land-use distributions, and topographies for all three domains were obtained from the WRF Preprocessing System, which is built into the modeling package and employs the U.S. Geological Survey topography and land-use categorization. Corresponding fields for the future state (LAKE experiment) were determined from the

TABLE 1. Modeling domains and corresponding horizontal and temporal resolutions employed in this study.

Domain (annotation)	Outermost (d01)	Medium (d02)	Innermost (d03)
Horizontal dimensions	891 km × 891 km	297 km × 297 km	120 km × 120 km
No. of grid points in the east–west direction	100	100	121
No. of grid points in the north–south direction	100	100	121
No. of grid points in the vertical direction	50	50	50
Horizontal step	9 km	3 km	1 km
Time step	30 s	10 s	3 s

TABLE 2. Selected physical parameterizations and numerical schemes. For further details, refer to Skamarock et al. (2008).

Parameterization/scheme	Selected option	Reference
Horizontal grid	Arakawa C grid staggering	
Microphysical scheme	Purdue Lin	Lin et al. (1983)
Longwave/shortwave radiation	Rapid Radiative Transfer Model	Mlawer et al. (1997)
Surface-layer scheme	Eta similarity	Janjić (2001)
Land surface model	5-layer thermal diffusion	
Planetary boundary layer scheme	Mellor–Yamada–Janjić	Mellor and Yamada (1982); Janjić (2001)
Cumulus parameterization	BMJ	Betts and Miller (1986); Janjić (1994)

fields obtained for the current state by replacing the data at grid squares corresponding to the location of the future lake with a water surface having an altitude of 550 m above sea level.

Selected numerical schemes and physical parameterizations are listed in Table 2. They were selected following past applications of the WRF model over domains elsewhere in Croatia (e.g., Belušić and Mahović 2009; Prtenjak et al. 2009, 2013; Kvakić 2012; Belušić et al. 2013). The same parameterizations/schemes were employed for all three domains. The exception is the Betts–Miller–Janjić (BMJ) parameterization (Betts and Miller 1986; Janjić 1994), which was used only for the d01 and d02 domains (cumulus physics were not parameterized for the finest domain).

The initial and boundary conditions for the outermost domain were taken from the National Centers for Environmental Prediction database (http://www.ncep.noaa.gov/), where the open-access results of Operational Model Global Tropospheric Analyses are available. Boundary conditions were taken from the Global Forecast System (GFS; http://rda.ucar.edu/datasets/ds083.2/) at horizontal and temporal resolutions of 1° and 6 h, respectively. In the vertical direction, 26 GFS mandatory levels ranging from 1000 to 10 hPa were employed.

Whereas lake surfaces were not resolved in domains d01 and d02, surface skin temperatures at the finest resolution (d03) were calculated for both the NO-LAKE and LAKE experiments using the freshwater lake model FLake (Mironov 2008). The FLake model is a lake parameterization module developed for the use in numerical weather prediction. It predicts the vertical structure of lake temperature over time scales from a few hours to years. The model is based on a two-layer parameterization of the evolving temperature profile and on the integral energy budget for the layers in question. FLake also has a snow–ice option, which was not employed in the present study. Namely, since data on ice and snow cover were not available, based on data observed at the measuring site closest to lakes (Gospić in Fig. 1b; see section 4a) we assumed that during simulated time intervals (section 3c) lakes were not frozen. Additionally, during the selected time intervals there were no snowfalls in the vicinity of the lakes. The FLake model was forced with the same dataset and at the same resolution as the WRF model. To avoid any spurious lake temperature oscillations, a spinup time of 1 yr was assumed. Modeled lake-surface temperatures (i.e., skin temperatures) were assimilated into WRF computations every sixth hour.

c. *Selection of simulated time intervals*

Real typical synoptic situations were selected to capture both the season (warm/cold) and the synoptic-scale pressure pattern (cyclonic/anticyclonic). Thus, four time intervals in total, during which the wider area of interest was under wintertime anticyclonic (WA), wintertime cyclonic (WC), summertime anticyclonic (SA), and summertime cyclonic (SC) conditions, were chosen (Table 3). Since greater amounts of precipitation and stronger winds are generally associated with the eastern and southern side of the cyclone compared with the northern and western side, when selecting WC and SC, we chose these two episodes for which the area of interest was found at the eastern and/or southern side of cyclone.

Lončar and Bajić (1994) investigated a 20-yr climatology of inland regions of Croatia. By analyzing surface synoptic charts they determined seasonal frequencies of days associated with 28 different weather types, where five among them are anticyclonic (the center of anticyclone, eastern, southern, western, and northern side of anticyclone), and four are cyclonic (the eastern, southern, western, and northern side of cyclone) (e.g., Klaić 2001). Whereas all five anticyclonic weather types are characterized by similar typical weather conditions, cyclonic weather types can be grouped into two groups. The first group (the eastern and southern side of a cyclone) is characterized by stronger winds and more intense precipitation, and, as already stated above, it is of the interest for the purpose of this study. The second group (the western and northern side of a cyclone) is characterized by weaker winds, and less intense precipitation. Based on results given for four seasons (Lončar and Bajić 1994), we estimate that the cold season (16 October–15 April) has about 19% of days associated with

TABLE 3. List of typical synoptic situations, short description of corresponding typical local weather conditions and simulated time intervals. All selected time intervals start and end at 1200 UTC.

Typical synoptic situation/annotation	Typical weather conditions	Selected time interval
Wintertime anticyclone/WA	Weak winds, clear skies, steadily falling temperatures over night and consequent frost and fog formation, no precipitation (except for occasional weak drizzle or snow grains produced by a fog).	2–4 Jan 2009
Wintertime cyclone/WC	Windy and cloudy with rain or snow.	30 Nov–2 Dec 2009
Summertime anticyclone/SA	Calm, clear, and fine weather; possible daytime formation of fine weather cumulus clouds; pronounced diurnal variation of the surface air temperature. Occasionally, because of local instabilities, cumulus clouds can develop into cumulonimbus clouds accompanied with local showers, hail and thunderstorms.	31 Jul–2 Aug 2010
Summertime cyclone/SC	Windy and cloudy with abundant rain.	26–28 May 2009

the first group of cyclonic weather types (i.e., eastern and southern side of a cyclone) and 43% of days associated with anticyclonic weather types. The warm season (16 April–15 October) has about 15% of days corresponding to the first group of cyclonic weather types and 33% days corresponding to anticyclonic weather types. Thus, weather conditions similar to conditions of selected episodes are expected to occur in approximately 62% of days during the cold season (i.e., 43% + 19%) and in approximately 48% of days during the warm season (i.e., 33% + 15%).

Representative synoptic situations were selected based on the surface synoptic diagnostic charts for Europe (not shown here). These charts are produced and archived daily by the Deutscher Wetterdienst every 6 h (0000, 0600, 1200, and 1800 UTC; the charts are available at http://www.wetter3.de/Archiv/archiv_dwd.html).

4. Results and discussion

a. Model verification

Although the WRF model has been applied worldwide (some references are given in section 2) as well as elsewhere in Croatia (e.g., Belušić and Mahović 2009; Prtenjak et al. 2009, 2013; Kvakić 2012; Belušić et al. 2013; Kuzmić et al. 2013), we inspected its performance at the finest resolution (1 km, domain d03) over the area of interest. Figures 2 and 3 show a comparison between the modeled and observed hourly mean values of available meteorological data (wind speed, wind direction, air temperature, and relative humidity) for four measuring sites (Gospić, Zavižan, Senj, and Rab; see Fig. 1b) during the simulated time intervals listed in Table 3. Table 4 shows mean absolute errors (MAEs) for the wind speed, wind direction, surface air temperature, and surface relative humidity. MAE was selected as appropriate measure of model performance based on the recommendation of Willmott and Matsuura (2005). It was calculated as in Hrust et al. (2009): $\mathrm{MAE} = (1/N)[\Sigma|(O_i - M_i)|]$, where O_i and M_i are observed and modeled values, respectively, and N is the number of pairs of the observed and modeled values. Specifically for the wind direction, possible artificial errors in calculation of MAE were eliminated by replacing $|(O_i - M_i)|$ with $[360° - |(O_i - M_i)|]$ if $|(O_i - M_i)|$ was initially greater than 180°. [For example, $O_i = 350°$ and $M_i = 4°$ produce artificially large absolute error of $|(O_i - M_i)| = 346°$, while the real absolute error is 14°, that is, $360° - |(O_i - M_i)|$.]

The surface-measured data were taken from the open access National Climatic Data Center database (available at http://www.ncdc.noaa.gov/). We note that measured data were frequently missing (viz., per particular measuring site, meteorological variable, and simulated synoptic setup between 24% and 69% of data were missing).

The model performance for the surface wind speed (Figs. 2a–d; Table 4) is comparable with the performance of other mesoscale meteorological models over other domains in Croatia (e.g., Klaić et al. 2003; Belušić and Klaić 2006; Klaić et al. 2009a; Tudor and Ivatek-Šahdan 2010). The agreement between modeled and measured wind speeds is generally better inland (Gospić and Zavižan, Figs. 2a and 2b, respectively; Table 4) compared with coastal measuring sites (Senj and Rab, Figs. 2c,d; Table 4). Better agreement for inland sites can, to a certain extent, be attributed to the model's spatial resolution, which, in the case of coastal sites, most likely results in misclassification of some land points as water points causing thus an overestimation of sea surface effects. Namely, modeled wind speeds at the coastal sites Senj and Rab are always higher than measured speeds (Figs. 2c and 2d, respectively), which is not the case for inland sites Gospić and Zavižan (Figs. 2a,b). Generally, higher speeds are expected above the sea surface because of weaker surface friction. Therefore,

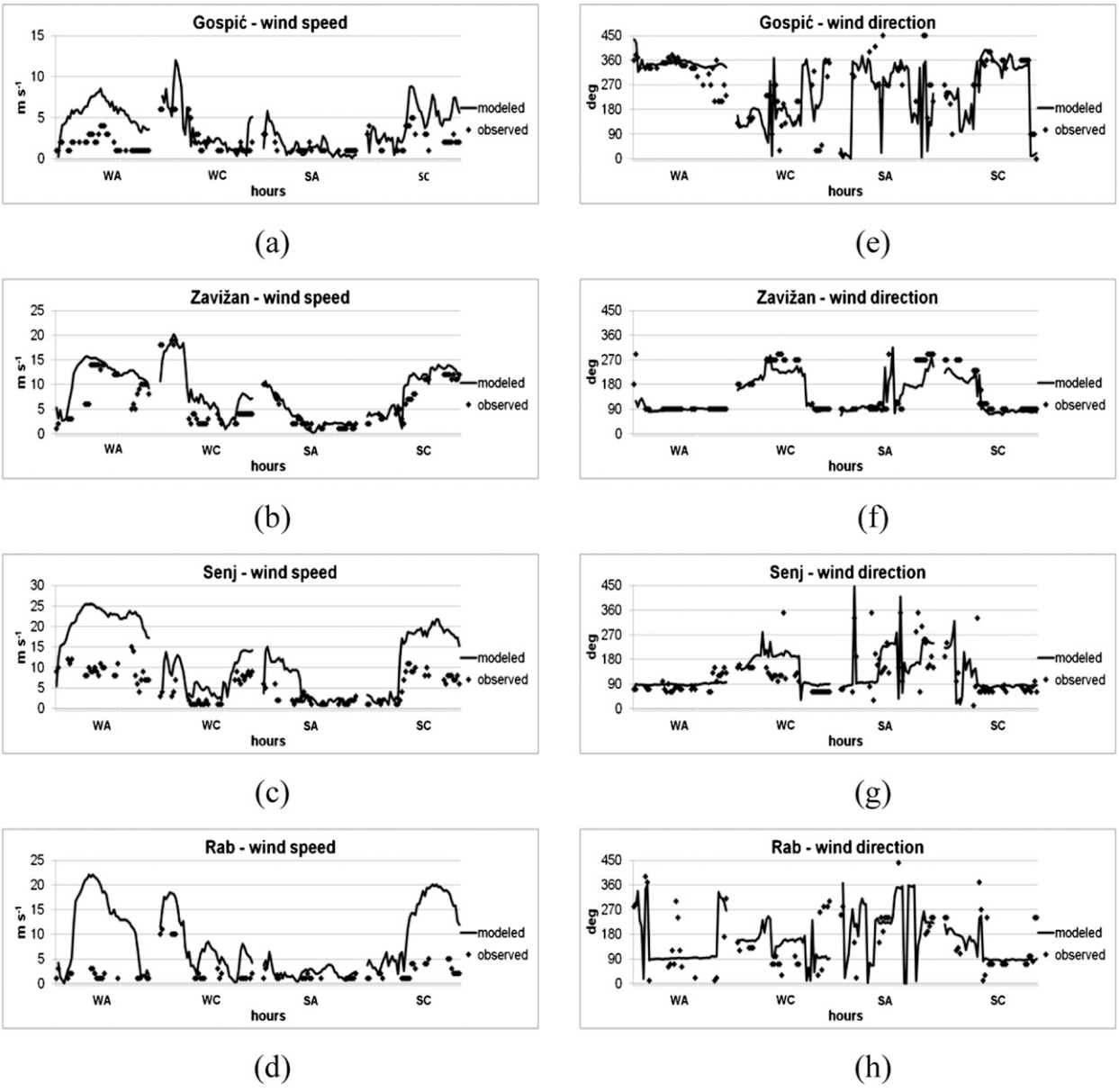

FIG. 2. Modeled (NO-LAKE) vs observed hourly mean surface (10 m AGL) (a)–(d) wind speed and (e)–(h) wind direction at the four measuring sites shown in Fig. 1b. Time intervals are denoted by WA, WC, SA, and SC. Note that some of the wind directions between 0° and 90° are enlarged by 360° to facilitate a visual comparison of measured and modeled values. (For example, a comparison of 5° and 350° would produce an artificially large discrepancy between these two values. Because of the circular nature of wind directions, the same can be expressed as 365° and 350°.)

we believe that as a result of resolution limits, the model overvalued the sea surface effects for coastal sites and thus overestimated the wind speeds.

Additionally, in cases of Senj and Rab (Figs. 2c and 2d, respectively), the discrepancy between the modeled and measured wind speed is partially caused by the already documented inadequate positions of measuring sites. Specifically, the measuring site in Senj is sheltered from winds blowing from the northeastern quadrant (Klaić et al. 2009b; Belušić et al. 2013), that is, from directions that correspond to bora winds (e.g., Yoshino 1976). Thus, real bora flows in Senj, particularly strong and severe boras, which are due to the east-northeastern local topography (direction ~70°), are substantially stronger than operationally measured winds (Klaić et al. 2009b). We note that the time intervals with the largest discrepancies between modeled and observed wind speeds in Senj (e.g., the entire WA and the last two-thirds

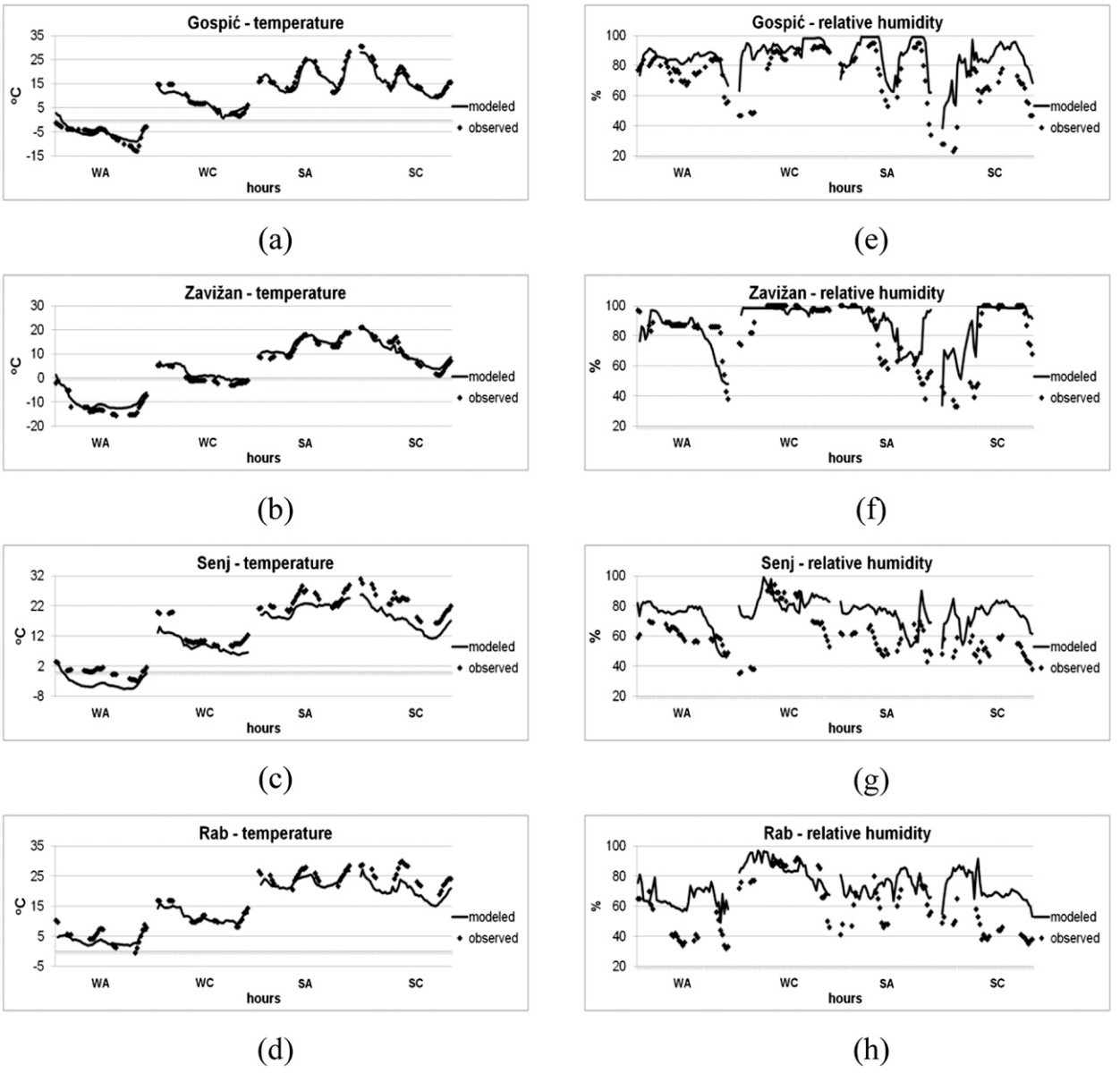

FIG. 3. Modeled (NO-LAKE) vs observed hourly mean surface (2 m AGL) (a)–(d) air temperature and (e)–(h) relative humidity of the air at the four measuring sites shown in Fig. 1b for WA, WC, SA, and SC.

of the SC episode in Fig. 2c) coincide with the time intervals with wind directions of ~70° (Fig. 2g), that is, with directions corresponding to the bora flow. Thus, we believe the model predicts the wind speed in Senj better than suggested by Fig. 2c. The anemometer in Rab, on the other hand, is sheltered from winds having directions between northeast and south (Belušić et al. 2013).

Last, considering all four measuring sites, we note that the wind speed pattern (increase and/or decrease of the wind speed with time) is well captured by the model. Additionally, as seen from the Figs. 2e–h, the modeled wind directions for all four sites generally agree reasonably well with the observed values.

Figure 3 shows the modeled versus measured hourly mean surface air temperature (Figs. 3a–d) and relative humidity (Figs. 3e–h) for the four investigated synoptic episodes. The predictions of temperature are particularly good for inland sites Gospić and Zavižan (Figs. 3a and 3b, respectively). The somewhat poorer prediction of temperatures in the case of Senj and Rab further corroborates our hypothesis that the model, because of resolution limitations, most likely misclassifies some

TABLE 4. Mean absolute errors for the wind speed (MAE_{speed}), surface air temperature (MAE_{temp}), and surface relative humidity (MAE_{RH}) and wind direction (MAE_{dir}) for investigated synoptic setups (Table 3). Number of pairs of measured and modeled values N employed in error calculations is given in parentheses.

Synoptic setup	MAE	Gospić	Zavižan	Senj	Rab
WA	MAE_{speed} ($m\,s^{-1}$)	3.70 (36)	3.10 (28)	13.04 (28)	10.77 (17)
WC	MAE_{speed} ($m\,s^{-1}$)	1.39 (28)	3.14 (28)	4.06 (28)	4.66 (19)
SA	MAE_{speed} ($m\,s^{-1}$)	0.78 (22)	0.86 (28)	2.94 (29)	1.10 (15)
SC	MAE_{speed} ($m\,s^{-1}$)	2.55 (27)	2.16 (27)	7.76 (28)	9.14 (23)
WA	MAE_{dir} (°)	36.84 (36)	8.88 (28)	22.08 (28)	62.71 (17)
WC	MAE_{dir} (°)	79.45 (28)	21.79 (28)	54.37 (29)	82.20 (19)
SA	MAE_{dir} (°)	66.90 (22)	41.37 (28)	69.72 (29)	45.42 (16)
SC	MAE_{dir} (°)	39.35 (27)	28.76 (27)	35.89 (28)	49.91 (23)
WA	MAE_{temp} (°C)	1.53 (36)	2.12 (28)	3.45 (28)	1.87 (22)
WC	MAE_{temp} (°C)	1.01 (29)	1.63 (28)	3.00 (29)	0.81 (22)
SA	MAE_{temp} (°C)	1.63 (28)	1.36 (28)	2.93 (28)	1.70 (22)
SC	MAE_{temp} (°C)	1.34 (28)	1.98 (27)	5.32 (28)	4.52 (22)
WA	MAE_{RH} (%)	7.88 (36)	7.94 (28)	11.01 (28)	19.39 (22)
WC	MAE_{RH} (%)	9.54 (29)	3.62 (28)	16.95 (29)	8.13 (22)
SA	MAE_{RH} (%)	11.84 (28)	17.96 (28)	18.94 (28)	13.56 (22)
SC	MAE_{RH} (%)	20.09 (28)	15.36 (27)	22.63 (28)	25.97 (22)

land points as water points and thus overestimates an influence of the sea. Namely, for the summertime anticyclone, when we generally expect pronounced diurnal variation of temperature and consequently, prominent diurnal temperature amplitude, modeled diurnal variations and amplitudes for Senj and Rab (SA episodes in Figs. 3c and 3d, respectively) are not so pronounced as observed. Similarly, better temperature predictions for inland compared with coastal sites were documented previously elsewhere over the Adriatic associated with the Aire Limitée Adaptation Dynamique Développement International (ALADIN) mesoscale model (Klaić et al. 2009a). The relative humidity (Figs. 3e–h) is well predicted for the inland sites, particularly for the wintertime (Table 4). For the coastal sites Senj and Rab (Figs. 3g and 3h, respectively; Table 4), the prediction is good for the wintertime cyclone (Rab) and wintertime anticyclone (Senj), while for the other time intervals it is somewhat poorer. We note however, that both the temperature pattern and the relative humidity pattern (increase and/or decrease in time) are well predicted by the model.

In summary, we conclude that the WRF model performed well over domain d03 for all four typical synoptic episodes. The agreement between the modeled and observed values was particularly good for inland sites (Gospić and Zavižan), which are both geographically closer (Fig. 1b) and climatologically more similar to the area where the future lake will be placed than the two coastal sites. Thus, we conclude that the WRF model can be applied to assess possible influences of the new inland lake on meteorological conditions above the neighboring areas.

b. *Modeled differences between LAKE and NO-LAKE experiments: Scalar fields*

Theoretically, the introduction of a water body instead of a solid surface can affect the water cycle budget, heat exchange at the surface, and surface friction. An increase of the quantity of water that is available for evaporation can increase the moisture flux from the surface and thus favor the formation of clouds and precipitation or fog. Changes in the moisture flux from the surface also affect other meteorological variables depending on moisture, such as the relative humidity of the air, the water vapor mixing ratio, the cloud mixing ratio, and the specific humidity. Because the WRF model does not produce a straightforward forecast of the fog, here we will analyze changes in the modeled cloud mixing ratio (CMR) within the 50-m-deep ground-based layer, where CMR is defined as a mass of cloud elements (droplets or ice crystals) per mass of dry air. High CMR values within the ground-based layer point to the presence of fog (a higher CMR implies denser fog, while no fog conditions require CMR = 0). The presence of fog should also be accompanied with high surface relative humidity values (at least approximately 90% or higher).

The introduction of the water surface also changes the radiation/absorption properties of the surface. In comparison with land, water has a high specific heat capacity and thus is heated by the absorption of solar radiation during the daytime (summer) at a much slower rate than land. Similarly, cooling of the water surface due to longwave radiation during the nighttime (winter) is also much slower than the cooling of the land. Accordingly, the

temperature of the air above the water surface is generally lower during the daytime (summer) relative to the temperature of the air above the land, while during the nighttime (winter), it is higher. Also, the water surface is smoother when compared with that of the land, thus producing less friction. Accordingly, lake construction could cause changes in the ambient wind field.

It is important to note that all possible effects of the future lake act simultaneously and that they mutually interact in a complex, nonlinear manner. For example, a change in the temperature field (caused by changes in the radiation/absorption properties of the surface) can change the ambient pressure field and, accordingly, the wind field. However, these changes in the wind field can modify advection (i.e., the transport of a property by the wind field) of other atmospheric properties, such as water vapor or temperature, which can then affect the wind field and other meteorological fields.

Differences in the modeled atmospheric fields in each grid point and for every hour of simulation were calculated by subtraction of the modeled value obtained for the current state (NO-LAKE) from the modeled value obtained for the future state (LAKE). The first 12 h of each simulation were considered as a prerun (thus, hereinafter these results were not analyzed). Accordingly, for each meteorological variable and each synoptic setup listed in Table 3, a total of 36 hourly output files were obtained. For the purposes of illustration, however, we show only snapshots of the modeled differences (Figs. 4–7). That is, we show some of the hours in which noticeable differences are present in at least two out of four meteorological fields (viz., CMR, relative humidity, wind speed, and temperature). The results are shown over a portion of domain d03 that surrounds lakes and that has an area of 50 km × 50 km. This area stretches downstream of the new lake over distances up to ~4*L*–6*L*.

The inspection of all output files for wintertime anticyclone mainly showed no difference between the LAKE and NO-LAKE results for CMR (Fig. 4a). Only occasionally and only over limited areas was the CMR for the LAKE experiment somewhat larger (up to at most 0.2 g kg^{-2}) than the CMR for the NO-LAKE experiment. Therefore, we conclude that the new lake would not substantially affect fog formation in the wintertime anticyclonic conditions. This conclusion is further corroborated by small differences in the surface relative humidity of the air. Namely, except for the very location of the new lake, the differences at all times are mainly within the range of ±5%. One such example is depicted in Fig. 4b. However, above the new lake the surface relative humidity under wintertime anticyclonic conditions would on the average be approximately 48% lower compared with the current NO-LAKE state. This result can be attributed to the wintertime increase of surface air temperature, which would occur above the new lake because of the replacement of land by a water body, which is also seen in Fig. 4d. The above is further corroborated with an inspection of modeled surface specific humidity fields (not shown here), which showed almost no difference between the LAKE and NO-LAKE surface specific humidity. (That is, the decrease in relative humidity was primarily produced by the increase in surface temperature.) The differences in precipitation amounts are also negligible (cf. Figs. 4e,f), which is in agreement with small changes in relative humidity over the entire 50 × 50 km^2 area. Nevertheless, LAKE experiment results show an north-northeast–south-southwest elongated band stretching from the southern tip of the lake, where accumulated precipitation is slightly (~1 mm) higher compared to the NO-LAKE experiment. This slight increase in accumulated precipitation near the lake for the LAKE experiment might be caused by an enhancement of the moist convection due to the lake effect. The same effect was already documented for lakes of comparable sizes (Laird et al. 2009, 2010). However, to confirm our hypothesis, further investigation of at least several WA episodes is needed.

As already discussed in the previous paragraph, under the wintertime anticyclonic conditions, the new lake would produce an increase of surface temperatures in the air above the lake. Such an increase (occasionally up to ~5°C) is found for every simulated hour. Moreover, south of the new lake a temperature increase of approximately 1°C frequently occurs over an elongated area stretching in the north–south direction (not shown here). Inspection of the wind field revealed that during the entire simulated interval, northern winds dominated over that area. These winds resulted in an advection of the warm air formed above the new lake toward the south and the consequent increase of the temperature in the region south of the lake for the LAKE experiment. Additionally, in several hours (4 out of 36) the temperature above the northern portion of the existing lake was at most 4°C lower in the LAKE when compared with the NO-LAKE experiment (Fig. 4d). As illustrated in Fig. 4c, the differences in the surface wind speed are generally low. When they are found, their values are at most up to ±2 m s^{-1}.

Figure 5 illustrates the differences between the LAKE and NO-LAKE experiment results for the summertime anticyclone. As seen from the entire set of results (here, we show only one hour in Fig. 5a), differences in the surface cloud mixing ratio are most frequently (in 15 out of 36 h of simulation) found above and/or within the vicinity of the lakes, where they occasionally range from −0.9 to 1.1 g kg^{-1}. However, we note that there is almost

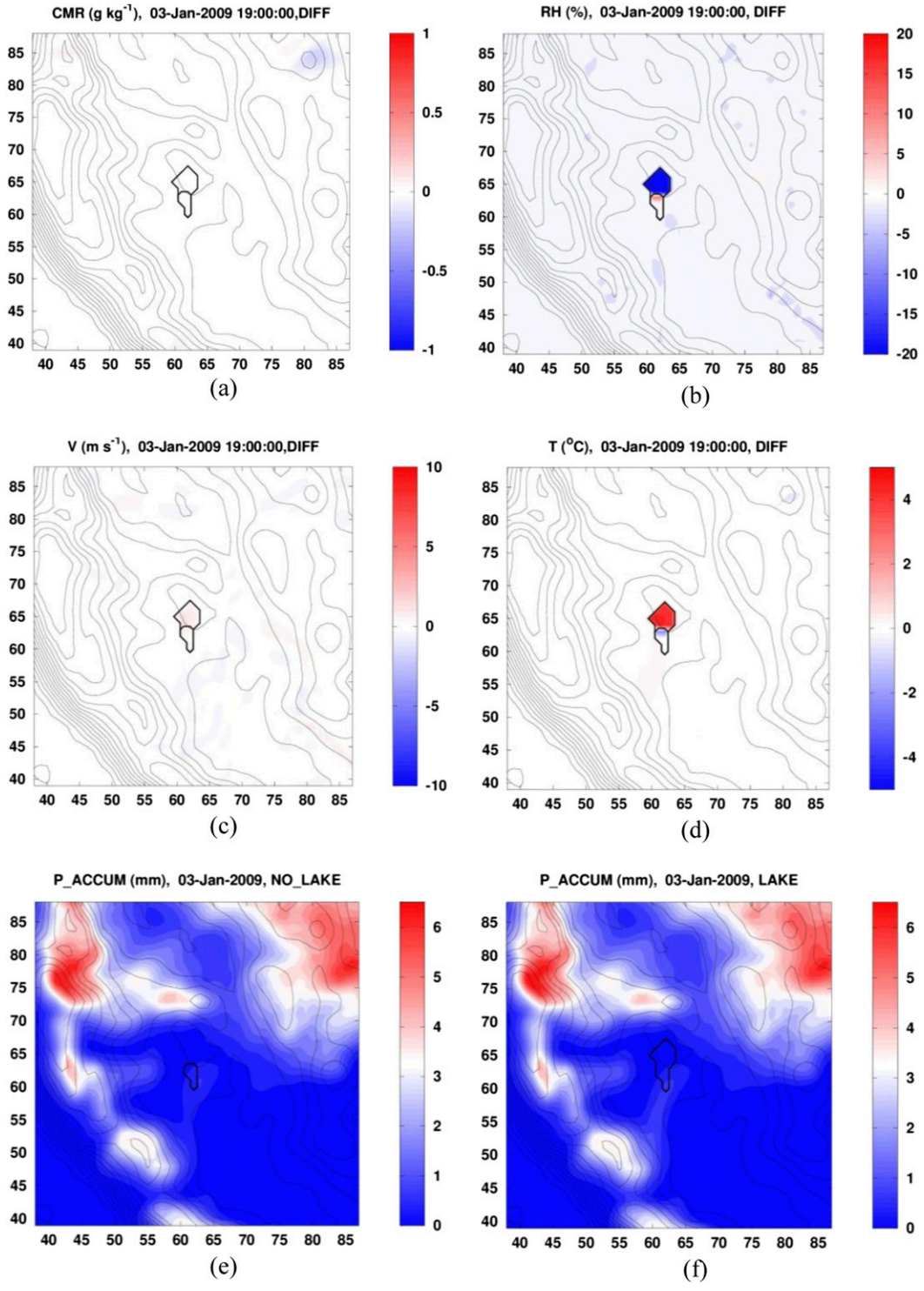

FIG. 4. WRF-modeled hourly mean differences between the future (LAKE) and current (NO-LAKE) states for WA at 1900 UTC 3 Jan 2009 for (a) surface cloud mixing ratio (first 50 m AGL; $g\,kg^{-3}$), (b) surface relative humidity (2 m AGL; %), (c) surface horizontal wind speed (10 m AGL; $m\,s^{-1}$), and (d) surface air temperature (2 m AGL; °C). (e),(f) Total precipitation (mm) accumulated over 36 h of simulation for the NO-LAKE and LAKE experiments, respectively. Axes display every fifth kilometer of the portion of the domain d03 (50 km × 50 km), which surrounds both lakes. Topography contours are shown for every 100 m, and lake borders are drawn in black.

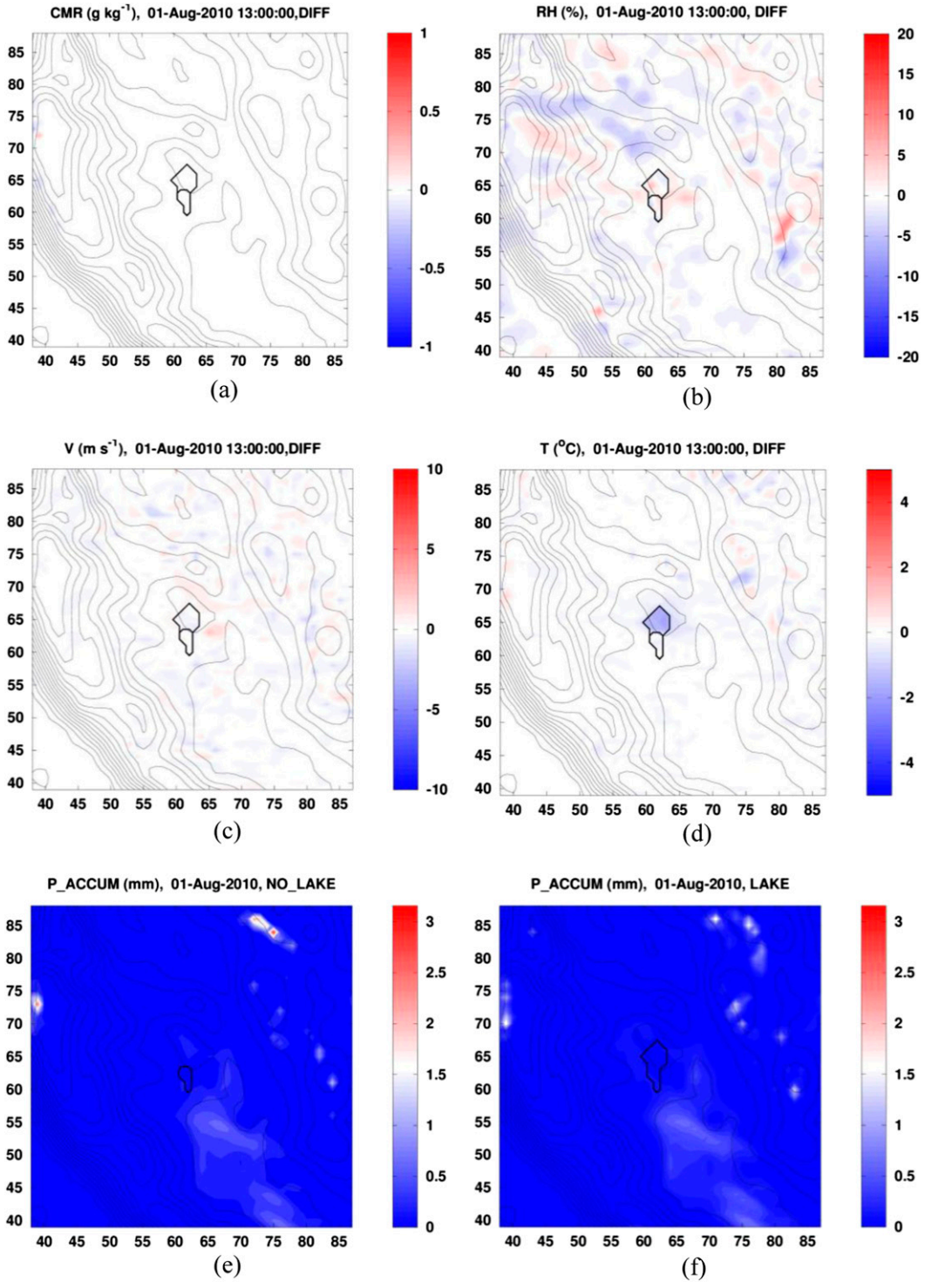

FIG. 5. As in Fig. 4, but for SA at 1300 UTC 1 Aug 2010.

no bias toward a general increase or decrease of CMR values in the LAKE conditions (the 36-h average difference between the LAKE and NO-LAKE CMR for the entire 50 km × 50 km, although negative, is only $-0.0019\,\mathrm{g\,kg^{-1}}$), that is, when differences exist, both positive and negative values of similar amounts always occur simultaneously above the inspected 50 km × 50 km area.

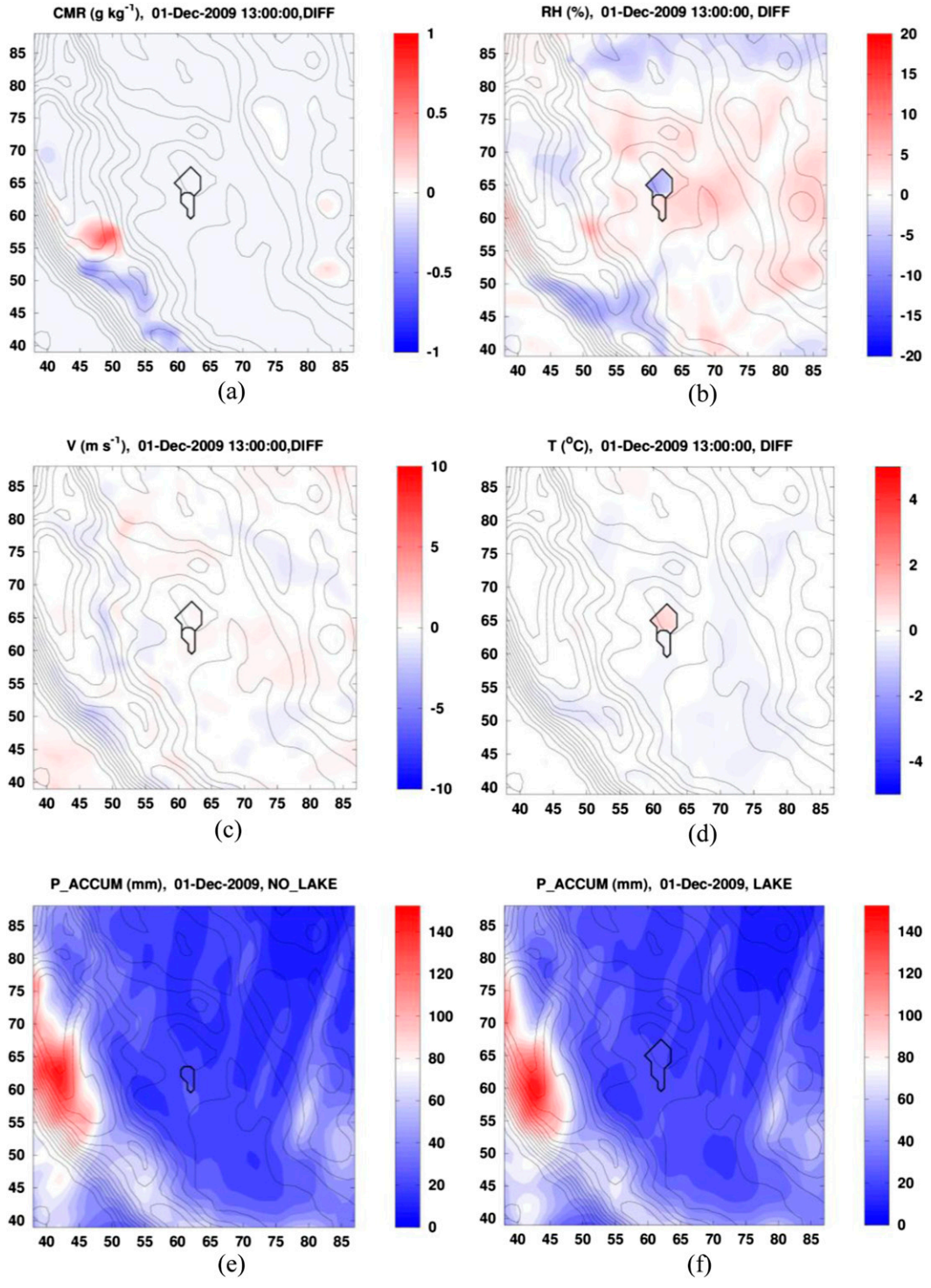

FIG. 6. As in Fig. 4, but for WC at 1300 UTC 1 Dec 2009.

The differences in the relative humidity (Fig. 5b) are within the range of ±20%. However, above the area of the new lake a persistent decrease is found in the LAKE conditions during the nighttime, or when the solar radiation is weak (early evening and morning hours) (not shown here). Again, such behavior can be attributed to the nighttime increase in temperature caused by the introduction of a water surface. Thus, the air above

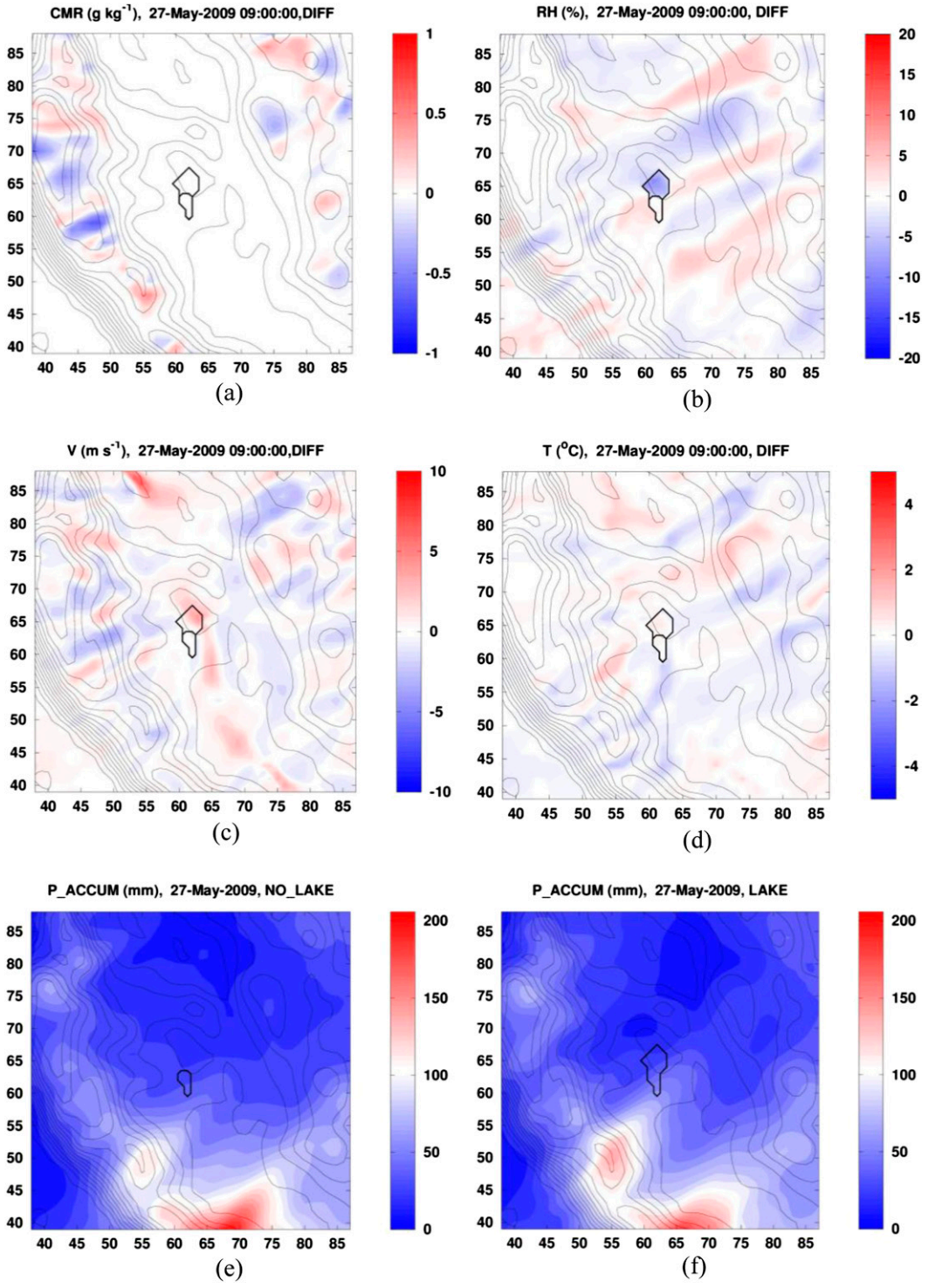

FIG. 7. As in Fig. 4, but for the SC at 0900 UTC 27 May 2009.

the lake would be warmer when compared with the current (NO-LAKE) state, and consequently, the relative humidity would be lower. Conversely, for daytime hours an increase in relative humidity is found above the lake (one such example is shown in Fig. 5b). Just as for the wintertime anticyclone, the dominant role of temperature over the specific humidity in changes of surface relative humidity was additionally corroborated by

inspection of surface specific humidity fields (not shown here). Similarly to the CMR behavior, apart from the area above the new lake, the fields of relative humidity differences also do not suggest any prominent bias toward a general increase or decrease of values (difference averaged over entire 50 km × 50 km area and over 36 h of simulation is −0.01%). In other words, both positive and negative values of similar amounts occur simultaneously throughout the simulated time interval.

Summertime anticyclonic conditions are generally characterized by fine and dry weather (see the typical weather conditions in Table 3). Thus, precipitation can occur only occasionally and only over a limited area, if local instabilities are established. Accordingly, weak precipitation intensities (up to approximately 1–2 mm h^{-1}) occurred only sporadically over small areas in some of the simulation hours for both LAKE and NO-LAKE experiment (not shown). Accordingly, both experiments resulted in very similar modeled fields of the total precipitation accumulated over 36 h of simulation (Figs. 5e,f).

The differences in the temperature fields are the highest above the new lake and within its vicinity (Fig. 5d), where they are between −3°C and +6°C. We note that positive and negative differences correspond to the nighttime and daytime, respectively. In other areas, these differences are always between −1.9°C and +2.6°C. Above the new lake, these differences are again caused by the change in the radiation/absorption properties of the surface. Thus, during the nighttime (daytime), the air in the LAKE experiment is warmer (cooler) compared with the NO-LAKE experiment.

The differences in surface wind speeds are generally low and are always within an interval between −2 m s^{-1} and +3 m s^{-1} (Fig. 5c). Again, we note the simultaneous occurrence of positive and negative differences of similar amounts, which suggests there is no prominent inclination toward generally higher or lower wind speeds in LAKE conditions.

Figure 6 illustrates differences in meteorological files for wintertime cyclonic conditions. Over the investigated area and over the entire simulated episode, differences in the cloud mixing ratio, if they are present, are within the range of ±1 g kg^{-1} (Fig. 6a). Again, most frequently, both positive and negative differences of similar magnitudes occur simultaneously over the investigated area.

If they are present, the differences in relative humidity are within the range from −29% to +21% (Fig. 6b). The most persistent differences are found in the air above the new lake—in all of the simulated hours, the relative humidity for the LAKE experiment is smaller than the NO-LAKE (−12% on the average). In other parts of the investigated area, both positive and negative values of similar amounts are found simultaneously.

For individual simulation hours, the differences in precipitation fields are mainly small (2–3 mm h^{-1}), except for 3 out of 36 inspected hours, when in some areas they were as high as approximately ±15 mm h^{-1} (not shown here). Accordingly, fields of precipitation accumulated over the 36-h simulation for the NO-LAKE and LAKE experiments are very similar (Figs. 6e,f). Additionally, the LAKE experiment did not provide any clear evidence of lake-effect precipitation event. Although we note a northward elongated band of increased accumulated precipitation stretching from the northern tip of the new lake (Fig. 6f; $x \approx 64$, $y \approx 66$), it is accompanied by the decrease of precipitation, which is found eastward and westward of the band.

Figure 6d illustrates differences in the surface air temperature fields. The most prominent is an increase of the temperature above the new lake, which is found in almost all hours and sometimes rises to approximately +5°C. A temperature increase above the new lake is expected because of wintertime influences of the water surface. In other areas, differences either do not exist or do not exceed ±1°C, except for 8 consecutive hours out of the total of 36, when at some localities, differences up to approximately ±3°C are found. We note that this time interval characterized by larger differences in the temperature fields nearly coincides with the time interval accompanied by larger differences in relative humidity fields (not shown here).

Figure 6c illustrates differences in the surface wind field due to construction of the new lake. Apart from several hours, when at some locations values up to approximately ±8 m s^{-1} occur, the differences are within the interval of ±2–3 m s^{-1}.

The results for the summertime cyclone are illustrated in Fig. 7. If they exist, the differences in the surface cloud mixing ratio (Fig. 7a) are between −0.8 and +0.6 g kg^{-1}. A persistent decrease of the relative humidity (up to −18%) above the new lake is observed in all 36 h (Fig. 7b). In other areas, the differences are within an interval of ±9%.

The differences in hourly precipitation fields are generally low (±2 mm h^{-1}), except for 7 consecutive hours starting at 1900 UTC 27 May 2009 (not shown here). During these 7 h, the differences are within an interval of ±15 mm h^{-1}. However, both positive and negative values of similar magnitudes again occur simultaneously. Fields of accumulated precipitation are generally similar, although we note an area centered at $x \approx 55$ and $y \approx 50$, where accumulated precipitation for the LAKE experiment is higher when compared with NO-LAKE results.

The differences in air temperatures are generally the most persistent above the new lake, where an increase (occasionally up to about +5°C) is found in 29 out of

TABLE 5. The modeled 36-h mean differences between the LAKE and NO-LAKE experiments four synoptic setups listed in Table 3 for the wind speed v, surface air temperature t, surface air pressure p, precipitation intensity P, surface cloud mixing ratio CMR, surface relative humidity RH, surface specific humidity Q, and moisture flux from the surface MF. Results are shown separately for the area above the new lake (11.55 km^2), the area surrounding the new lake (2488.45 km^2), and the entire 50 km × 50 km area, respectively. For v, t, p, and RH the differences that are greater than standard instrument accuracies are in boldface type.

Synoptic setup	v (m s^{-1})	t (°C)	p (hPa)	P (mm h^{-1})	CMR (g kg^{-1})	RH (%)	Q (g kg^{-1})	MF (g m^{-2} s^{-1})
				Area above the new lake				
WA	**0.57**	**4.04**	−0.01	−0.01	0.0000	**−48.5**	0.01	0. 03
SA	**0.22**	**2.03**	−0.01	−0.04	−0.0560	**−6.4**	0.80	−0. 01
WC	**0.27**	**1.87**	−0.03	1.51	−0.1221	**−11.5**	0.16	0. 01
SC	**0.52**	**2.05**	0.01	1.21	−0.0192	**−7.8**	−0.10	0. 02
				Area surrounding the new lake				
WA	0.00	0.01	0.00	0.01	0.0000	−0.1	0.00	0. 00
SA	0.01	0.01	0.00	0.00	−0.0017	−0.4	0.01	0. 00
WC	0.02	0.03	−0.01	−0.30	−0.0109	−0.2	0.01	0. 00
SC	−0.01	−0.03	0.01	0.43	−0.0001	0.1	−0.01	0. 00
				Entire 50 km × 50 km area				
WA	0.01	0.03	0.00	0.01	−0.0001	−0.3	0.00	0. 00
SA	0.01	0.02	0.00	0.00	−0.0019	−0.1	0.01	0. 00
WC	0.02	0.04	−0.01	−0.29	−0.0115	−0.3	0.01	0. 00
SC	−0.01	−0.02	0.01	0.43	−0.0002	0.1	−0.01	0. 00

36 h. In other parts of the investigated area, the differences are within the range of ±2.5°C (Fig. 7d).

Figure 7c illustrates modeled differences in the wind fields under summertime cyclonic conditions. The highest differences are within the range of about ±10 m s^{-1}. Again, no pronounced bias toward a general increase or decrease of the wind speed above the investigated area is found because both positive and negative values of similar magnitudes occurred simultaneously.

Finally, Table 5 summarizes the modeled changes of meteorological variables averaged over the 36 h of the simulated synoptic setup. In addition to the results obtained for the variables shown in Figs. 4–7, the results for the surface air pressure p, surface specific humidity Q, and moisture flux from the surface MF are listed. For each simulated time interval, average changes of the meteorological values are separately shown for the area above the new lake, the area surrounding the lake, and the entire 50 km × 50 km area.

As expected, the largest differences in meteorological fields due to construction of the new lake are obtained for the area above the new lake, while in the remaining area they are substantially smaller. Furthermore, as seen in Table 5, apart from the area above the new lake, the modeled differences are below the accuracies of the measurement instruments. [For example, the accuracy of current Vaisala (Helsinki, Finland) sensors is ±0.12°C for the air temperature, ±0.1 m s^{-1} for the wind speed (sonic), ±0.1 hPa for the air pressure, and ±1% for the relative humidity.]

In the end, we inspected temporal variations of differences between the LAKE and NO-LAKE experiments results. While cyclonic setups did not result in any diurnal variations of differences between the LAKE and NO-LAKE experiments, anticyclonic setups clearly exhibited diurnal patterns for the relative humidity and temperature (not shown here). For both variables and both seasons these differences were larger during the nighttime compared to the daytime. However, these diurnal patterns were not accompanied by similar patterns of other meteorological variables.

c. *Modeled differences between the LAKE and NO-LAKE experiments: Thermally driven circulations*

Recent findings of Asefi-Najafabady et al. (2012) and Crosman and Horel (2012) showed that lake circulations can establish over small lakes despite their sizes. Therefore, here we will inspect the following: 1) did such circulations exist during investigated episodes, and if they did, 2) were they affected by the presence of the new lake?

As with other local thermal circulations (sea and land breezes, up- and downslope winds, river winds, etc.), lake breezes generally establish under summertime fair weather conditions (e.g., Harris and Kotamarthi 2005). On the other hand, strong synoptic forcing can completely prohibit their development (e.g., Asefi-Najafabady et al. 2012). Among the four episodes investigated in the present study, only SA was associated with weak synoptic forcing (i.e., with conditions favorable for the lake-breeze establishment), while the remaining three episodes were accompanied with stronger background winds (not shown here). During the SA episode, modeled differences between land and lake

temperature (2 m above the surface) were at most up to ~3°–5°C.

Figure 8 shows modeled surface winds at different times during the SA episode for the NO-LAKE and LAKE experiments, respectively. Although employed model resolution is not fine enough to capture full details of the onshore and offshore flows for such small lakes, we note that during the daytime a flow divergence (suggesting lake breezes) is found above the lake surface for both the NO-LAKE (Figs. 8a,c,e) and LAKE (Figs. 8b,d,f) experiments. Conversely, during the nighttime, a flow convergence above the lake surface (suggesting land breezes) is found for the NO-LAKE (Figs. 8g,i) and LAKE experiments (Fig. 8h—southern portion of lake, and Fig. 8j). Additionally, modeled wind fields reproduced diurnal, thermally induced slope winds, which are generally established above south-facing slopes of hills and mountains under the same conditions of weak synoptic forcing (Reuten et al. 2005; Klaić et al. 2009a). Namely, daytime winds for the NO-LAKE experiment (Figs. 8a,c,e) show upslope flow in the area having x coordinate approximately between 61 and 67, and y coordinate approximately between 66 and 70. During the nighttime, downslope, weaker winds are frequently found in the same area (Figs. 8g,i). As expected, up- and downslope winds are also found in the same area for the LAKE experiment.

Considering the differences between the LAKE and NO-LAKE wind fields, modeled surface winds over the new lake (LAKE) were frequently stronger than winds above the same area associated with solid surface (NO-LAKE) (see, e.g., point $x = 63$, $y = 66$ in Figs. 8c,d or point $x = 63$, $y = 64$ in Figs. 8i,j). This is expected because of weaker surface friction over the water compared to solid surface. However, it is interesting that during the daytime a slight increase in the wind speed for the LAKE compared to the NO-LAKE experiment was occasionally found outside the new lake area. Specifically, it was found in the area associated with upslope winds (see, e.g., point $x = 63$, $y = 68$ in Figs. 8a,b, point $x = 65$, $y = 66$ in Figs. 8c,d, and, again, point $x = 65$, $y = 66$ in Figs. 8e,f). During the nighttime, an increase in the wind speed for the LAKE experiment compared to the NO-LAKE experiment was also found in the same area (see, e.g., point $x = 65$, $y = 66$ in Figs. 8g,h and, again, in Figs. 8i,j). However, the nighttime increase in the wind speed was smaller than the daytime increase.

5. Conclusions

The investigation of possible changes in surface meteorological fields (viz., the wind speed, air temperature, air pressure, precipitation amount, cloud mixing ratio, relative humidity, and moisture flux from the surface) caused by the construction of a small man-made lake (surface area of 11.55 km^2 and maximum fetch distance of approximately 5 km) was performed by application of the mesoscale meteorological model WRF to the four typical synoptic setups (wintertime anticyclone, summertime anticyclone, wintertime cyclone, and summertime cyclone). Results of the model verification exhibit generally better model performance over inland, compared to coastal areas. Similar results were already documented for other mesoscale models (e.g., Klaić et al. 2009a). Somewhat poorer model performance for coastal sites can generally arise because of coarse resolution or inadequate representation of air–sea interactions in the model. In addition, specifically for coastal winds in the present study, the discrepancies between modeled and measured values were partially caused by inadequate (sheltered) positions of both anemometers.

Possible changes in meteorological fields were inspected within the 50 km × 50 km area encompassing the new lake. This area corresponds to distances up to ~4L–6L downstream of the new lake. The investigation revealed that the largest changes were to the surface air temperature and relative humidity. Not surprisingly, the strongest influences of the new lake are found in the air above the lake. In the remaining parts of the investigated 50 km × 50 km area, the assessed 36-h mean changes in meteorological fields due to the new lake were for all variables at least an order of magnitude smaller than the accuracy of standard meteorological sensors. However, for individual simulations hours, large changes in meteorological fields were occasionally found over limited portions of the area surrounding the lake. Nevertheless, in such cases, no prominent bias toward the general increase or decrease of meteorological values was found because both positive and negative values of similar amounts occurred simultaneously. Additionally, except for the area above the new lake, the magnitudes of individual changes were the most frequently larger for cyclonic compared with anticyclonic setups.

According to the model results, the surface air temperature above the lake increased for wintertime anticyclone (on average by +4.0°C), wintertime cyclone (+1.9°C), and summertime cyclone (+2.1°C). This increase was present at almost all times of the simulated episodes. However, for the summertime anticyclone, the temperature change caused by the new lake depended on the time of day. Accordingly, during the daytime and nighttime, the temperature decreased (~−0.1°C) and increased (~+4.2°C), respectively, while it increased on average (+2°C).

The relative humidity of the air above the new lake generally decreased. Changes were the largest for the

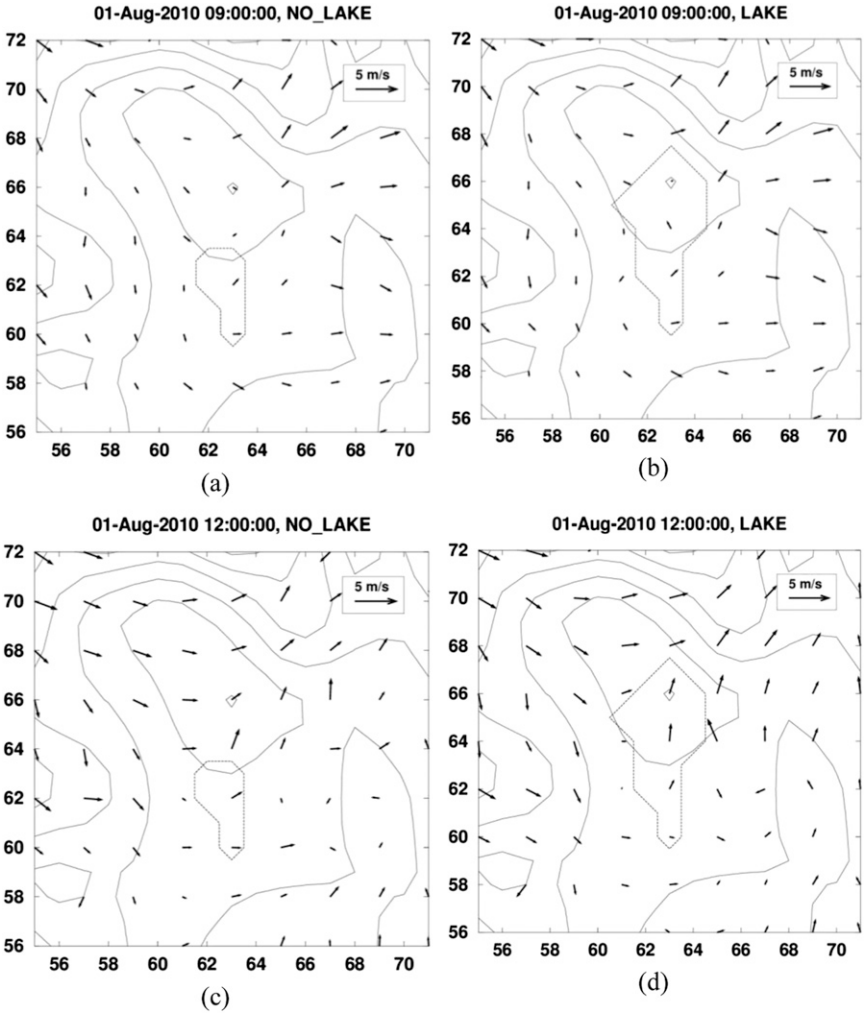

FIG. 8. A closer view of the modeled (d03) surface winds (10 m AGL) around lakes for SA at different times (UTC; local mean solar time is UTC +1). Results for the (left) NO-LAKE and (right) LAKE experiments. Topography contours are shown for every 50 m. Lake borders are shown with dotted lines. Axes display every second kilometer.

wintertime anticyclone (on average −48.5%). For other synoptic setups they were as follows: wintertime cyclone (−11.5%), summertime cyclone (−7.8%), and summertime anticyclone (−6.8%).

A small increase in the surface wind speed above the new lake was obtained for all four setups. This increase was for wintertime episodes approximately +0.6 and $+0.3\,\mathrm{m\,s^{-1}}$ for the anticyclone and cyclone, respectively. For summertime episodes it was approximately $+0.2\,\mathrm{m\,s^{-1}}$ (anticyclone) and $+0.5\,\mathrm{m\,s^{-1}}$ (cyclone).

While absolute differences between the LAKE and NO-LAKE surface temperature and relative humidity exhibited diurnal variations for both anticyclonic setups (being larger during the nighttime compared with the daytime), such patterns were not found for cyclonic episodes. This is not surprising since atmospheric variables associated with cyclones generally do not follow diurnal patterns.

Although the employed model resolution was not fine enough to capture details in the lake circulation over such a small lake, the daytime surface airflow divergence and the nighttime surface airflow convergence, which were found above the lake, suggest the existence of such thermally induced circulation under weak synoptic forcing. The surface airflow divergence/convergence was associated with small differences between lake and land temperature, which were at most up to ~3°–5°C. This is in accordance with recent findings of Asefi-Najafabady et al. (2012). Namely, based on observational data the authors showed that lake-breeze circulations can be produced by

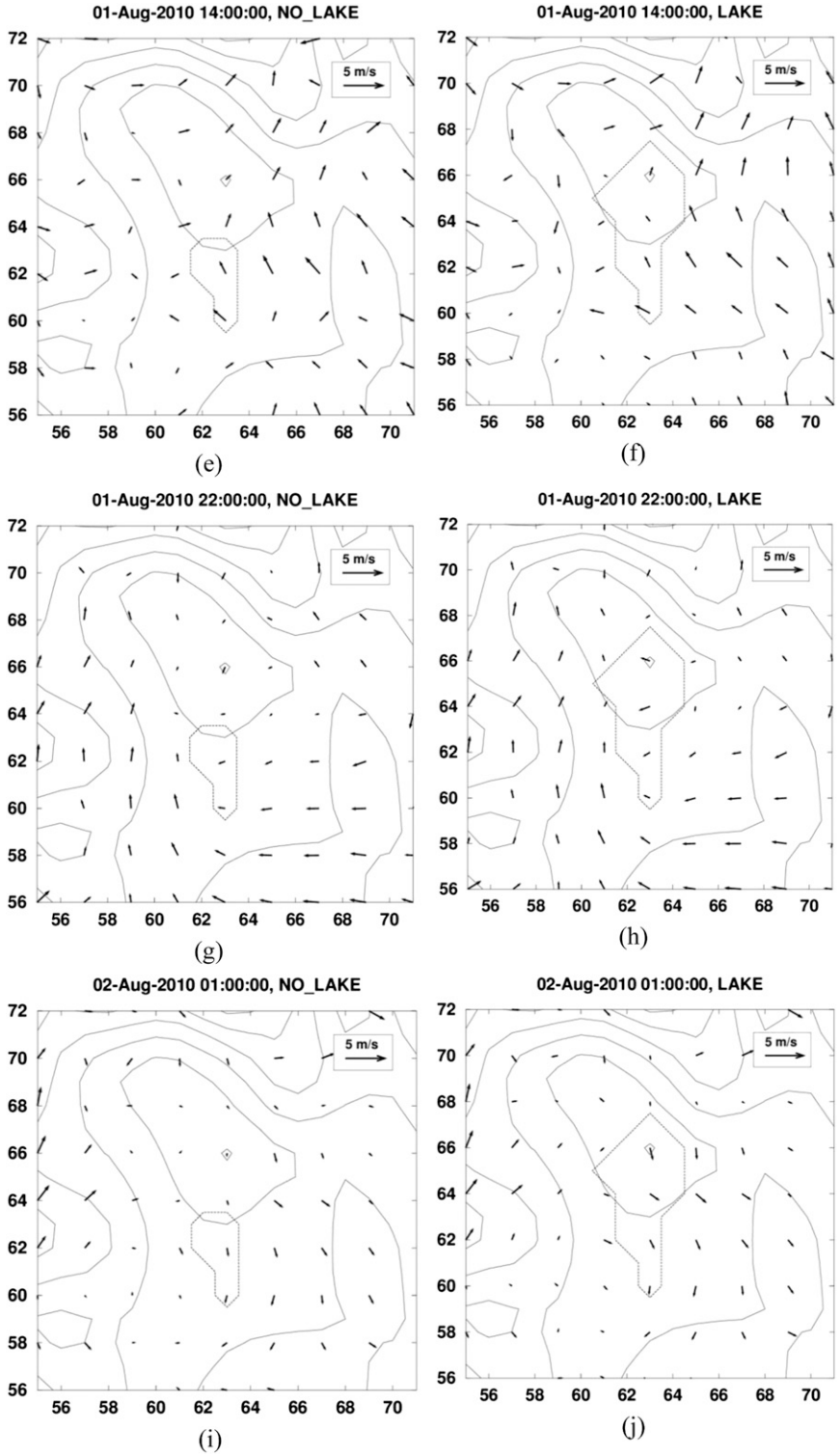

FIG. 8. (*Continued*)

a small lake of comparable size and that they can be driven by differences between land and lake temperature of a few degrees Celsius.

Additionally, our results suggest a slight increase in the net slope winds due to construction of the new lake. In other words, lake circulation that is produced by the new lake interplays with the diurnal, thermally induced slope winds established above south facing slopes of nearby topographic obstacles. Since both these thermally induced circulations have similar wind directions throughout the day, their superposition acts to enhance the net slope flow. Similar interplay but between the sea/land breezes and slope winds was already described by others (e.g., Melas et al. 2000; Caballero and Lavagnini 2002; Klaić et al. 2009a).

In future work, a numerical modeling study at finer spatial resolution (~100 m) would be desirable to investigate full details of both the lake circulation over such a small lake and its interplay with the slope winds. This would require appropriate representation of the atmospheric boundary layer, that is, large-eddy simulations nested with the WRF model.

A slight increase in accumulated precipitation, which was found in the areas above and nearby the new lake for the wintertime anticyclone episode and is possibly associated with lake-effect precipitation, also deserves further exploration. Moreover, a couple of recent studies (Laird et al. 2009, 2010) showed that lake-effect precipitation events do occur over lakes of comparable sizes. We note, however, that such investigations should include a larger number of wintertime episodes.

Last, we emphasize that this study of four cases focuses on short-term influences of the new lake on ambient atmospheric fields. However, long-term effects resulting from accumulation of slightly biased differences between the LAKE and NO-LAKE atmospheric fields over time are possible. Assessment of such long-term influences requires a multiyear climatological examination, which is beyond the scope of this study.

Acknowledgments. We are very grateful to three anonymous reviewers for their valuable suggestions. Elvira Horvatić Viduka of Ekonerg, Zagreb, provided us with details on lake geometries. The study was supported by the Croatian Ministry of Science, Education and Sport (Grant 119-1193086-1323).

REFERENCES

Alcott, T. I., W. J. Steenburgh, and N. F. Laird, 2012: Great Salt Lake–effect precipitation: Observed frequency, characteristics, and associated environmental factors. *Wea. Forecasting,* **27,** 954–971, doi:10.1175/WAF-D-12-00016.1.

Antonić, O., D. Hatic, J. Krian, and D. Bukovec, 2001: Modelling groundwater regime acceptable for the forest survival after the building of the hydro-electric power plant. *Ecol. Modell.,* **138,** 277–288, doi:10.1016/S0304-3800(00)00408-7.

Asefi-Najafabady, S., K. Knupp, J. R. Mecikalski, and R. M. Welch, 2012: Radar observations of mesoscale circulations induced by a small lake under varying synoptic-scale flows. *J. Geophys. Res.,* **117,** D01106, doi:10.1029/2011JD016194.

Bazgeer, S., P. K. Sharma, R. K. Mahey, S. S. Hundal, and A. Sood, 2008: Assessment of land use changes using remote sensing and GIS and their implications on climatic variability for Balachaur watershed in Punjab, India. *Desert,* **12,** 139–147.

Belušić, D., and Z. B. Klaić, 2006: Mesoscale dynamics, structure and predictability of a severe Adriatic bora case. *Meteor. Z.,* **15,** 157–168, doi:10.1127/0941-2948/2006/0116.

——, and N. S. Mahović, 2009: Detecting and following atmospheric disturbances with a potential to generate meteotsunamis in the Adriatic. *Phys. Chem. Earth,* **34,** 918–927, doi:10.1016/j.pce.2009.08.009.

——, M. Hrastinski, Ž. Večenaj, and B. Grisogono, 2013: Wind regimes associated with a mountain gap at the northeastern Adriatic coast. *J. Appl. Meteor. Climatol.,* **52,** 2089–2105, doi:10.1175/JAMC-D-12-0306.1.

Betts, A. K., and M. J. Miller, 1986: A new convective adjustment scheme. Part II: Single column tests using GATE wave, BOMEX, ATEX and arctic air-mass data sets. *Quart. J. Roy. Meteor. Soc.,* **112,** 693–709, doi:10.1002/qj.49711247308.

Biondić, B., R. Biondić, and F. Dukarić, 1998: Protection of karst aquifers in the Dinarides in Croatia. *Environ. Geol.,* **34,** 309–319, doi:10.1007/s002540050283.

Bogunović, M., Ž. Vidaček, and S. Husnjak, cited 2013: Soil classification for the needs of spatial planning in Croatia. European Soil Bureau Research Rep. 7, 63–67. [Available online at http://eusoils.jrc.ec.europa.eu/esdb_archive/eusoils_docs/esb_rr/n07_ESBResRep07/205Husnjak.pdf.]

Caballero, R., and A. Lavagnini, 2002: A numerical investigation of the sea breeze and slope flows around Rome. *Nuovo Cimento,* **25C,** 287–304.

Coniglio, M. C., K. L. Elmore, and J. S. Kain, 2010: Evaluation of WRF model output for severe weather forecasting from the 2008 NOAA Hazardous Weather Testbed spring experiment. *Wea. Forecasting,* **25,** 408–427, doi:10.1175/2009WAF2222258.1.

Cordeira, J. M., and N. F. Laird, 2008: The influence of ice cover on two lake-effect snow events over Lake Erie. *Mon. Wea. Rev.,* **136,** 2747–2763, doi:10.1175/2007MWR2310.1.

Crosman, E. T., and J. D. Horel, 2010: Sea and lake breezes: A review of numerical studies. *Bound.-Layer Meteor.,* **137,** 1–29, doi:10.1007/s10546-010-9517-9.

——, and ——, 2012: Idealized large-eddy simulations of sea and lake breezes: Sensitivity to lake diameter, heat flux and stability. *Bound.-Layer Meteor.,* **144,** 309–328, doi:10.1007/s10546-012-9721-x.

Dale, V. H., R. A. Efroymson, and K. L. Kline, 2011: The land use–climate change–energy nexus. *Landscape Ecol.,* **26,** 755–773, doi:10.1007/s10980-011-9606-2.

Foley, J. A., and Coauthors, 2005: Global consequences of land use. *Science,* **309,** 570–574, doi:10.1126/science.1111772.

Harris, L., and V. R. Kotamarthi, 2005: The characteristics of the Chicago lake breeze and its effects on trace particle transport: Results from an episodic event simulation. *J. Appl. Meteor.,* **44,** 1637–1654, doi:10.1175/JAM2301.1.

Hernández, J. L., S. Hwang, F. Escobedo, A. H. Davis, and J. W. Jones, 2012: Land use change in central Florida and sensitivity

analysis based on agriculture to urban extreme conversion. *Wea. Climate Soc.,* **4,** 200–211, doi:10.1175/WCAS-D-11-00019.1.

Horvath, K., D. Koracin, R. Vellore, J. Jiang, and R. Belu, 2012: Sub-kilometer dynamical downscaling of near-surface winds in complex terrain using WRF and MM5 mesoscale models. *J. Geophys. Res.,* **117,** D11111, doi:10.1029/2012JD017432.

Hrust, L., Z. B. Klaić, J. Križan, O. Antonić, and P. Hercog, 2009: Neural network forecasting of air pollutants hourly concentrations using optimised temporal averages of meteorological variables and pollutant concentrations. *Atmos. Environ.,* **43,** 5588–5596, doi:10.1016/j.atmosenv.2009.07.048.

Janjić, Z. I., 1994: The step-mountain eta coordinate model: Further developments of the convection, viscous sublayer and turbulence closure schemes. *Mon. Wea. Rev.,* **122,** 927–945, doi:10.1175/1520-0493(1994)122<0927:TSMECM>2.0.CO;2.

——, 2001: Nonsingular implementation of the Mellor–Yamada level 2.5 scheme in the NCEP Meso Model. NCEP Office Note 437, 61 pp.

Klaić, Z. B., 2001: Weather types and traffic accidents. *Coll. Antropol.,* **25,** 245–254.

——, T. Nitis, I. Kos, and N. Moussiopoulos, 2002: Modification of the local winds due to hypothetical urbanization of the Zagreb surroundings. *Meteor. Atmos. Phys.,* **79,** 1–12, doi:10.1007/s703-002-8225-z.

——, D. Belušić, I. H. Bulić, and L. Hrust, 2003: Mesoscale modeling of meteorological conditions in the lower troposphere during a winter stratospheric ozone intrusion over Zagreb, Croatia. *J. Geophys. Res.,* **108,** 4720, doi:10.1029/2003JD003878.

——, Z. Pasarić, and M. Tudor, 2009a: On the interplay between sea-land breezes and Etesian winds over the Adriatic. *J. Mar. Syst.,* **78,** S101–S118, doi:10.1016/j.jmarsys.2009.01.016.

——, A. D. Prodanov, and D. Belušić, 2009b: Wind measurements in Senj—Underestimation of true bora flows. *Geofizika,* **26,** 245–252.

Kuzmić, M., X.-M. Li, B. Grisogono, I. Tomažić, and S. Lehner, 2013: TerraSAR-X observations of the northeastern Adriatic bora: Early results. *Acta Adriat.,* **54,** 13–26.

Kvakić, M., 2012: An impact of physical parameterization in the mesoscale model on the simulated interaction between sea breeze and deep convection (in Croatian). M.S. thesis, Department of Geophysics, Faculty of Science, University of Zagreb, 52 pp.

Laird, N. F., D. A. R. Kristovich, and J. E. Walsh, 2003a: Idealized model simulations examining the mesoscale structure of winter lake-effect circulations. *Mon. Wea. Rev.,* **131,** 206–221, doi:10.1175/1520-0493(2003)131<0206:IMSETM>2.0.CO;2.

——, J. E. Walsh, and D. A. R. Kristovich, 2003b: Model simulations examining the relationship of lake-effect morphology to lake shape, wind direction and wind speed. *Mon. Wea. Rev.,* **131,** 2102–2111, doi:10.1175/1520-0493(2003)131<2102:MSETRO>2.0.CO;2.

——, R. Sobash, and N. Hodas, 2009: The frequency and characteristics of lake-effect precipitation events associated with the New York State Finger Lakes. *J. Appl. Meteor. Climatol.,* **48,** 873–886, doi:10.1175/2008JAMC2054.1.

——, ——, and ——, 2010: Climatological conditions of lake-effect precipitation events associated with the New York State Finger Lakes. *J. Appl. Meteor. Climatol.,* **49,** 1052–1062, doi:10.1175/2010JAMC2312.1.

Lin, Y.-L., R. D. Farley, and H. D. Orville, 1983: Bulk parameterization of the snow field in a cloud model. *J. Climate Appl. Meteor.,* **22,** 1065–1092, doi:10.1175/1520-0450(1983)022<1065:BPOTSF>2.0.CO;2.

Lončar, E., and A. Bajić, 1994: Weather types in Croatia (in Croatian). *Hrvat. Meteor. Čas.,* **29,** 31–41.

Melas, D., A. Lavagnini, and A.-M. Sempreviva, 2000: An investigation of the boundary layer dynamics of Sardinia island under sea-breeze conditions. *J. Appl. Meteor.,* **39,** 516–524, doi:10.1175/1520-0450(2000)039<0516:AIOTBL>2.0.CO;2.

Mellor, G. L., and T. Yamada, 1982: Development of a turbulence closure model for geophysical fluid problems. *Rev. Geophys. Space Phys.,* **20,** 851–875, doi:10.1029/RG020i004p00851.

Mironov, D. V., 2008: Parameterization of lakes in numerical weather prediction. Description of a lake model. COSMO Tech. Rep. 11, Deutscher Wetterdienst, Offenbach am Main, Germany, 41 pp. [Available online at http://www.cosmo-model.org/content/model/documentation/techReports/docs/techReport11.pdf.]

Mlawer, E. J., S. J. Taubman, P. D. Brown, M. J. Iacono, and S. A. Clough, 1997: Radiative transfer for inhomogeneous atmosphere: RRTM, a validated correlated-*k* model for the longwave. *J. Geophys. Res.,* **102,** 16 663–16 682, doi:10.1029/97JD00237.

Nicod, J., 2003: A little contribution to the karst terminology: Special or aberrant cases of poljes? *Acta Carsol.,* **32,** 29–39.

Notaro, M., A. Zarrin, S. Vavrus, and V. Bennington, 2013: Simulation of heavy lake-effect snowstorms across the Great Lakes Basin by RegCM4: Synoptic climatology and variability. *Mon. Wea. Rev.,* **141,** 1990–2014, doi:10.1175/MWR-D-11-00369.1.

Payer, M., J. Desrochers, and N. F. Laird, 2007: A lake-effect snowband over Lake Champlain. *Mon. Wea. Rev.,* **135,** 3895–3900, doi:10.1175/2007MWR2031.1.

Prtenjak, M. T., A. Jeričević, L. Kraljević, I. H. Bulić, T. Nitis, and Z. B. Klaić, 2009: Exploring atmospheric boundary layer characteristics in a severe SO_2 episode in the north-eastern Adriatic. *Atmos. Chem. Phys.,* **9,** 4467–4483, doi:10.5194/acp-9-4467-2009.

——, ——, Z. B. Klaić, A. Alebić-Juretić, and I. H. Bulić, 2013: Atmospheric dynamics and elevated ozone concentrations in the northern Adriatic. *Meteor. Appl.,* **20,** 482–496, doi:10.1002/met.1312.

Reuten, C., D. G. Steyn, K. B. Strawbridge, and P. Bovis, 2005: Observations of the relation between upslope flows and the convective boundary layer in steep terrain. *Bound.-Layer Meteor.,* **116,** 37–61, doi:10.1007/s10546-004-7299-7.

Sills, D. M. L., J. R. Brook, I. Levy, P. A. Makar, J. Zhang, and P. A. Taylor, 2011: Lake breezes in the southern Great Lakes region and their influence during BAQS-Met 2007. *Atmos. Chem. Phys.,* **11,** 7955–7973, doi:10.5194/acp-11-7955-2011.

Skamarock, W. C., and J. B. Klemp, 2008: A time-split nonhydrostatic atmospheric model for weather research and forecasting applications. *J. Comput. Phys.,* **227,** 3465–3485, doi:10.1016/j.jcp.2007.01.037.

——, and Coauthors, 2008: A description of the Advanced Research WRF version 3. NCAR Tech. Note NCAR/TN-475+STR, 113 pp. [Available online at http://www.mmm.ucar.edu/wrf/users/docs/arw_v3.pdf.]

Tudor, M., and S. Ivatek-Šahdan, 2010: The case study of bura of 1st and 3rd February 2007. *Meteor. Z.,* **19,** 453–466, doi:10.1127/0941-2948/2010/0475.

Vavrus, S., M. Notaro, and A. Zarrin, 2013: The role of ice cover in heavy lake-effect snowstorms over the Great Lakes basin as simulated by RegCM4. *Mon. Wea. Rev.,* **141,** 148–165, doi:10.1175/MWR-D-12-00107.1.

Willmott, C. J., and K. Matsuura, 2005: Advantages of the mean absolute error (MAE) over the root mean square error (RMSE) in assessing average model performance. *Climate Res.,* **30,** 79–82, doi:10.3354/cr030079.

Workoff, T. E., D. A. R. Kristovich, N. F. Laird, R. LaPlante, and D. Leins, 2012: Influence of the Lake Erie overlake boundary layer on deep convective storm evolution. *Wea. Forecasting,* **27,** 1279–1289, doi:10.1175/WAF-D-11-00076.1.

Wright, D. M., D. J. Posselt, and A. L. Steiner, 2013: Sensitivity of lake-effect snowfall to lake ice cover and temperature in the Great Lakes region. *Mon. Wea. Rev.,* **141,** 670–689, doi:10.1175/MWR-D-12-00038.1.

Yoshino, M. M., 1976: *Local Wind Bora.* University of Tokyo Press, 289 pp.

Zaninović, K., and Coauthors, 2008. *Klimatski atlas Hrvatske/Climate atlas of Croatia 1961–1990, 1971–2000*. Državni hidrometeorološki zavod, Zagreb, 200 pp.